Remote Sens. **2010**, *2*, 2571-2583; doi:10.3390/rs2112571

OPEN ACCESS

Remote Sensing

ISSN 2072-4292

www.mdpi.com/journal/remotesensing

Article

Long-Term Volcanic Activity at Shiveluch Volcano: Nine Years of ASTER Spaceborne Thermal Infrared Observations

Adam Carter *,† **and Michael Ramsey**

Department of Geology and Planetary Science, University of Pittsburgh, Pittsburgh, PA 15260, USA; E-Mail: mramsey@pitt.edu

* Author to whom correspondence should be addressed; E-Mail: carteradam09@gmail.com; Tel.: +1-412-624-8772; Fax: +1-412-624-3914.

† Currently at ExxonMobil, Houston, TX, USA.

Received: 27 September 2010; in revised form: 15 November 2010 / Accepted: 16 November 2010 / Published: 17 November 2010

Abstract: Shiveluch (Kamchatka, Russia) is the most active andesitic volcano of the Kuril-Kamchatka arc, typically exhibiting near-continual high-temperature fumarolic activity and periods of exogenous lava dome emplacement punctuated by discrete large explosive eruptions. These eruptions can produce large pyroclastic flow (PF) deposits, which are common on the southern flank of the volcano. Since 2000, six explosive eruptions have occurred that generated ash fall and PF deposits. Over this same time period, the Advanced Spaceborne Thermal Emission and Reflection Radiometer (ASTER) instrument has been acquiring image-based visible/near infrared (VNIR), short wave infrared (SWIR) and thermal infrared (TIR) data globally, with a particular emphasis on active volcanoes. Shiveluch was selected as an ASTER target of interest early in the mission because of its frequent activity and potential impact to northern Pacific air transportation. The north Pacific ASTER archive was queried for Shiveluch data and we present results from 2000 to 2009 that documents three large PF deposits emplaced on 19 May 2001, 9 May 2004, and 28 February 2005. The long-term archive of infrared data provides an excellent record on the changing activity and eruption state of the volcano.

Keywords: Shiveluch; volcanic hazards; remote sensing; thermal infrared; pyroclastic flow deposits

---

1. Introduction

1.1. Shiveluch Volcano

Shiveluch Volcano (also known as Sheveluch) is located at 56.65°N, 161.36°E on the Kamchatka peninsula of eastern Russia (Figure 1). It lies isolated in the lowland area of the Central Kamchatka depression and is the northernmost of 29 potentially active volcanoes on the peninsula [1]. The volcano is comprised of two sectors: Old and Young Shiveluch [2-4])—the summit of Old Shiveluch is 3,283 m above sea level (a.s.l.), whereas the summit of Young Shiveluch is approximately 2,800 m a.s.l. The activity at Young Shiveluch is composed of multiple extrusive andesite lava domes and thick (up to 100 m) lava flows [5]. Within the Holocene (last 10,000 years), at least 60 explosive eruptions have occurred at this location [6]. Ponomareva *et al.* [6] provide a detailed account of activity spanning the 1964–2004 time period.

Figure 1. Field photographs of Shiveluch summit showing the southern flank of the volcano, the active lava dome, and the large PF deposits. **(A)** Ground-based photograph taken March 2009 by Y. Demyanchuk looking northeast. **(B)** Helicopter-based photograph of the 2005 PF deposit taken August 2005 by M. Ramsey looking east. Active dome at the time of the images is shown by the arrows.

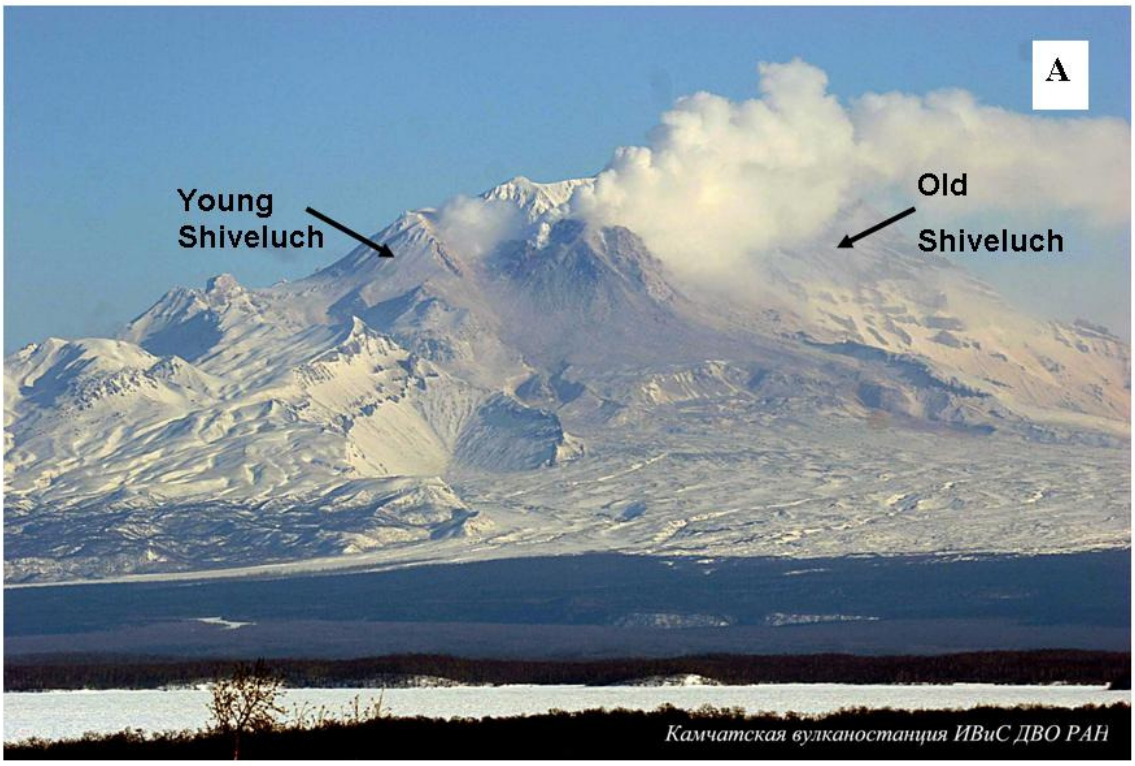

Figure 1. *Cont.*

Catastrophic slope failures of the lava dome and summit structure have been common at Shiveluch, occurring approximately 10,000, 5,700, 3,700, 2,600, 1,600, 1,000, 600 BP, 1964 AD, and producing debris avalanches deposits that cover much of the floor of the breached caldera [2,7]. The 1964 eruption produced a Plinian eruption column and 0.8 cubic kilometres of juvenile material [7]. The first significant explosion occurred on 7 May 1964, following strong, spasmodic volcanic tremor [5]. The eruption column reached a height of 4.5 km a.s.l. and was dispersed to the northwest [8]. Smaller, yet still significant, explosive eruptions have occurred since 1964 with the largest producing a 24,800 km^2 PF deposit on 27 February 2005 [2].

Since 1994 Kamchatka has been monitored by the Kamchatka Volcano Eruption Response Team (KVERT) and assisted by the Alaska Volcano Observatory's (AVO) routine satellite monitoring [9]. The time period of interest for this study was 2000–2009, which corresponds to the start of ASTER observations of Shiveluch. In 2004, a new collaborative program was initiated between NASA, AVO and KVERT that integrates the low spatial/high temporal resolution satellite data from the Moderate Resolution Imaging Spectroradiometer (MODIS) and the Advanced Very High Resolution Radiometer (AVHRR) as a detection trigger for scheduling and ASTER observation [10]. The MODIS and AVHRR data have been routinely used by AVO to monitor activity of any volcano in the North Pacific region. The integration of ASTER into this monitoring program has been highly successful both in increasing the overall number of ASTER images and the subsequent science that comes from these data of the active Kamchatka volcanoes [11-15].

1.2. The ASTER Urgent Request Protocol (URP) for Volcano Monitoring

The ASTER sensor collects image data of reflected and emitted energy in the VNIR region in three wavelength channels (0.56–0.81 μm) at 15 m/pixel spatial resolution, in the SWIR region in six wavelength channels (1.65–2.40 μm) at 30 m/pixel spatial resolution, and in the TIR region in five wavelength channels (8.29–11.32 μm) at 90 m/pixel spatial resolution [16,17]. However, beginning in May 2007 the SWIR data contained higher amounts of noise and saturated values due to a failure of the SWIR cryocooler. The SWIR data became completely saturated after January 2009 and are no longer useable. Useable ASTER data are processed into higher-level data products from geometrically and radiometrically corrected level 1 data [16]. The ASTER sensor maintains an observation schedule of regular acquistions of all the world's active volcanoes [18]. As of June 2009, over 96,000 distinct ASTER scenes have been collected for the 964 most active volcanoes, which is an average frequency of 5 daytime and 6 nighttime observations per volcano per year. However, for Shiveluch this average is much higher (13 daytime and 17 nighttime) resulting in at least one ASTER image of the volcano every 12 days on average. This higher frequency is a function of the location of Shiveluch coupled with specific ASTER data acquisition programs.

Active volcanoes of Kamchatka, specifically Bezymianny and Shiveluch were selected early on in the mission as high priority case studies for the ASTER sensor as part of a research investigation by the University of Pittsburgh (UP) and AVO [10,13,19], Because of the high latitude of Kamchatka, the temporal frequency of ASTER improves from the nominal 16 day repeat time at the equator to an average of 5 days. This frequency coupled with the high levels of varied activity at these volcanoes made them ideal targets for increased acquisitions.

The volcanic activity seen in these increased observations led to the development of two NASA-funded projects that linked the routine, near-real time satellite monitoring carried out by AVO in the North Pacific region with the ASTER scheduling system for rapid scheduling, tasking, and data availability. A previously-developed algorithm by AVO, which automatically processes thermal anomalies from low (1 km) spatial resolution AVHRR data [9], was significantly improved to minimize false positive detections and allow for the triggering of an automatic urgent-priority ASTER image. This urgent request protocol (URP) is one of the unique characteristics of ASTER, providing a limited number of emergency observations per day, typically at a much-improved temporal resolution and quicker turn around bypassing processing in Japan, which can add several days to a week to receive the processed data. The ongoing multi-agency research and operational collaboration has proven to be highly successful. AVO serves as the primary source for status information on volcanic activity and collaboration with IVS/KVERT is also maintained. Once a volcano is identified as having increased thermal output in the AVHRR or MODIS data, ASTER is automatically tasked for observation of that volcano at the next available opportunity. After the data are acquired, scientists at all the agencies have immediate access to the images, with the primary science analysis carried out at the University of Pittsburgh. Results of that analysis are disseminated back to AVO and KVERT, who have the primary monitoring and alerting responsibilities to other agencies. Results are also disseminated to the global volcanological community through email mailing lists. This system does not have the ability to provide real-time data on an eruption, but does greatly improve the nominal ASTER

scheduling/acquisition/processing pathway and can provide syn- and post-eruption data that can assist in future volcano monitoring and prediction [11,12].

1.3. Objectives

The primary objective of this study was to assess the statistical and scientific results of nine years of ASTER observations for Shiveluch and to provide an account of thermal activity for low-level degassing, lava dome growth, explosions, and the emplacement of PF deposits. The ASTER instrument was launched in December 1999 and the first data acquired for scientific studies were in March 2000, thereby overlapping the last four years of the time period described in Dirksen *et al.* [5] for Shiveluch. From 2000 to 2009, six large explosive eruptions have occurred interspersed with high levels of activity such as dome growth, lava flow emplacement, and hot rock avalanches. The correlation of ASTER-derived temperature data to explosive, effusive, non explosive, and periods of no detectable activity were investigated. The specific focus was on the three PF-forming eruption that occurred on 19 May 2001, 9 May 2004, and 28 February 2005, each of which was imaged by ASTER shortly after the PF emplacement.

2. Methods

Using the publically-available Japanese *ASTER image database for volcanoes* website [20] all available ASTER data of the Shiveluch region were identified, ordered using the U.S. *NASA Warehouse Inventory Search Tool (WIST)* [21] and later analyzed. Cloud-free, night time TIR images were then ordered as level 2 (L2) surface kinetic temperature and emissivity data products (Table 1). The TIR sensor is sensitivity to temperatures that range from −73 to 97 °C, and has a 1–2 °C detection threshold with a ±3 K radiometric accuracy, making it ideal to observe both low-level fumarolic activity as well as hotter thermal features resulting from magmatic activity [16]. With hotter activity, the TIR pixels are at risk of saturation, which occurs during periods of increased dome growth at Shiveluch. However, it is rare to have the pixel-integrated brightness temperature of a 90 m^2 pixel greater than 97 °C due to the presence and mixing of cooler surfaces. In the event of saturated pixels, data from the SWIR or VNIR region can be analyzed because of their much higher surface temperatures. Clearly with more recent data, the SWIR bands are not useable resulting in a loss of data and accuracy of the thermal analysis. ASTER L2 kinetic temperature data derived from the atmosphercially-corrected TIR data were used for this study [22]. The average background temperature for each image was calculated from a non-active 20 km^2 area (50 × 50 TIR pixels) at a similar elevation to the active dome. This non-active region was carefully selected so it had similar solar heating conditions, rock type and ground cover as the thermally-elevated pixels. Because the ASTER data are always acquired at the same local time and the rock types are similar, we do not expect the radiant temperature to be markedly affected by thermophysical variations such as thermal inertia, thermal conductivity or heat capacity [23]. The average thermal background temperature value was subtracted from the thermally-anomalous pixels, thereby removing any bias for seasonal warming/cooling. Temperature data were also retrieved from the AVHRR image archive [9]. These data were used as a comparison to the ASTER-derived temperature data over the same periods, as well

as to analyze the statistics of AVHRR data over the area and assess the sensitivity in triggering ASTER image requests.

Table 1. ASTER data used within this study. T_{BG} = background temperature, T_{max} = maximum scene temperature.

Date	Day/Night	ASTER Granule ID	Mean T_{BG} (Celsius)	T_{max} above T_{BG} (Celsius)
19-May-01	night	SC:AST_L1A.003:2003153825	1.24	107.81
04-Jun-01	night	SC:AST_L1A.003:2003226401	−3.59	40.14
15-Jul-01	night	SC:AST_L1A.003:2004160600	2.81	101.64
16-Jan-02	night	SC:AST_L1A.003:2006261433	−26.48	122.33
24-Feb-02	night	SC:AST_L1A.003:2028982939	−23.64	126.29
29-Apr-02	night	SC:AST_L1A.003:2027028338	−9.32	105.57
02-Jul-02	night	SC:AST_L1A.003:2007616604	6.87	102.18
25-Jul-02	night	SC:AST_L1A.003:2007919716	−23.04	87.99
07-Nov-02	night	SC:AST_L1A.003:2009058095	−13.62	83.17
11-Dec-02	night	SC:AST_L1A.003:2010414584	−22.47	21.42
18-May-03	night	SC:AST_L1A.003:2013901971	−3.20	108.95
21-Jul-03	night	SC:AST_L1A.003:2015471404	6.10	23.75
10-Mar-04	night	SC:AST_L1A.003:2021737898	−21.63	81.38
26-Mar-04	night	SC:AST_L1A.003:2022152144	−18.42	41.67
18-Apr-04	night	SC:AST_L1A.003:2022690296	−17.22	37.07
11-May-04	night	SC:AST_L1A.003:2023494312	−7.12	116.17
29-Mar-05	night	SC:AST_L1A.003:2028324137	−17.14	112.59
29-Apr-05	day	SC:AST_L1A.003:2028759514	−18.68	19.43
20-Jun-06	night	SC:AST_L1A.003:2034709250	4.42	14.23
14-Aug-06	night	SC:AST_L1A.003:2036141373	12.55	29.10
14-Nov-07	night	SC:AST_L1A.003:2062570037	−17.08	122.33
18-Feb-08	night	SC:AST_L1A.003:2071616266	−27.22	117.87
06-Apr-08	night	SC:AST_L1A.003:2073165383	−14.17	79.62
24-May-08	night	SC:AST_L1A.003:2068876087	−2.83	79.08
27-Jul-08	night	SC:AST_L1A.003:2066053085	8.36	93.39
06-Nov-08	day	SC:AST_L1A.003:2067619803	−22.62	127.97
19-Jan-09	night	SC:AST_L1A.003:2069994240	−28.12	111.87

3. Data Analysis and Results

3.1. Eruption Descriptions

The May 2001 explosive eruption generated a lava flow on the previous dome and a collapsing flow front of hot rock avalanches (Figure 2). The associated PF deposit travelled 12 km confined within a channel, which was the topographic low-point south of the summit dome. This suggests that the flow had a high bulk density (e.g., block-rich) as it became focused within the channel. On 19 May 2001 ASTER imaged Shiveluch and revealed a high-temperature (several pixels > 100 °C) thermal anomaly centred on the central summit region. This temperature was above the saturation point for the ASTER TIR indicating a large area of lava at/or near magmatic temperatures was exposed. The thermal

anomaly was located near the dome front, where surface or near-surface dome growth was likely occurring. In addition, the channelized PF deposit was less than two TIR pixels (180 m) wide.

The May 2004 eruption produced an ASTER TIR thermal anomaly over the majority of the Young Shiveluch crater, with over 30 saturated pixels on the southern part of the lava dome. They formed a linear thermal anomaly over 1 km in length, strongly suggesting the presence of a lava flow with hot rock avalanches occurring on the south part of the dome. The high number of saturated pixels on the south part of the dome indicated that magmatic temperatures were once again present at the time of the ASTER image acquisition.

The PF deposit produced during this eruption was divided into two main channels with the majority of the deposit focused in the western lobe (Figure 2). This fanned out at lower slope angles and dissipated into smaller channels. The maximum distance travelled by the PF was 9.5 km to the south, with the branch point of the two lobes occurring at 2.7 km from the dome. The western-most lobe was areally the largest and widest (maximum 2.3 km in width). The central western lobe contained the warmest temperatures found in the PF deposit. This hotter zone terminated around 7 km from the dome and was correlates with the results found by [14] who linked this hotter core with a higher density, less vesicular, block-rich deposit that formed from a collapse of the dome hours to days after the PF deposit was emplaced.

The ASTER image acquired on 29 March 2005 contained the largest thermal anomalies ever recorded by ASTER in Kamchatka. The 28 February explosive eruption at Shiveluch was the largest at the volcano since the 1964 event that produced a vast debris avalanche deposit to the south of the volcano. The thermal anomaly observed at the dome was almost circular in plan-view, 800 m in diameter, and had one distinct lobe to the southwest, around 1.8 km from the dome summit. Although the summit anomaly was the hottest in the scene, the highest amount of thermally-elevated pixels were located on the large (19 km long and up to 1.8 km wide at a distance of 15.8 km from the dome) PF deposit that was emplaced on the southwest flank (Figure 2). This deposit initially travelled south and was contained in the same channel as the May 2001 PF deposit. However, at about the same distance (~12 km) where the 2001 deposit terminated, the March 2005 deposit fanned out into a wide plain and travelled another ~10 km to the west. The westernmost front of the deposit contained four major lobes all oriented west. The image acquired was one month after the eruption, and so temperatures were considerably lower in general than the other two deposits. However, a distinct thermal anomaly remained detectable for the next year.

3.2. Multittemporal Image of the Dome and PF Deposit Region

The three ASTER images from 19 May 2001, 11 May 2004, and 29 March 2005 were assembled into a multi-temporal image composite displayed in red, green, and blue, respectively to show the areal extent, thermal intensity, and overlapping relationships of the thermal anomalies generated by the explosive eruptions on 19 May 2001, 9 May 2004, and 28 February 2005 (Figure 2). Each eruption produced a unique thermal signature due to lava flow emplacement and rock falls at the summit dome, and the large pyroclastic flow deposits on the southern flank. Figure 2 shows the utility of such multi-temporal image composites when studying multiple overlapping (and cooling) PF deposits.

Figure 2. ASTER multi-temporal temperature image composite from 19 May 2001 (red), 11 May 2004 (green), and 29 March 2005 (blue) that highlights the extent (area) and magnitude (intensity of the colour) of the warm deposits. These deposits were generated by the explosive eruptions on 19 May 2001, 9 May 2004, and 28 February 2005.

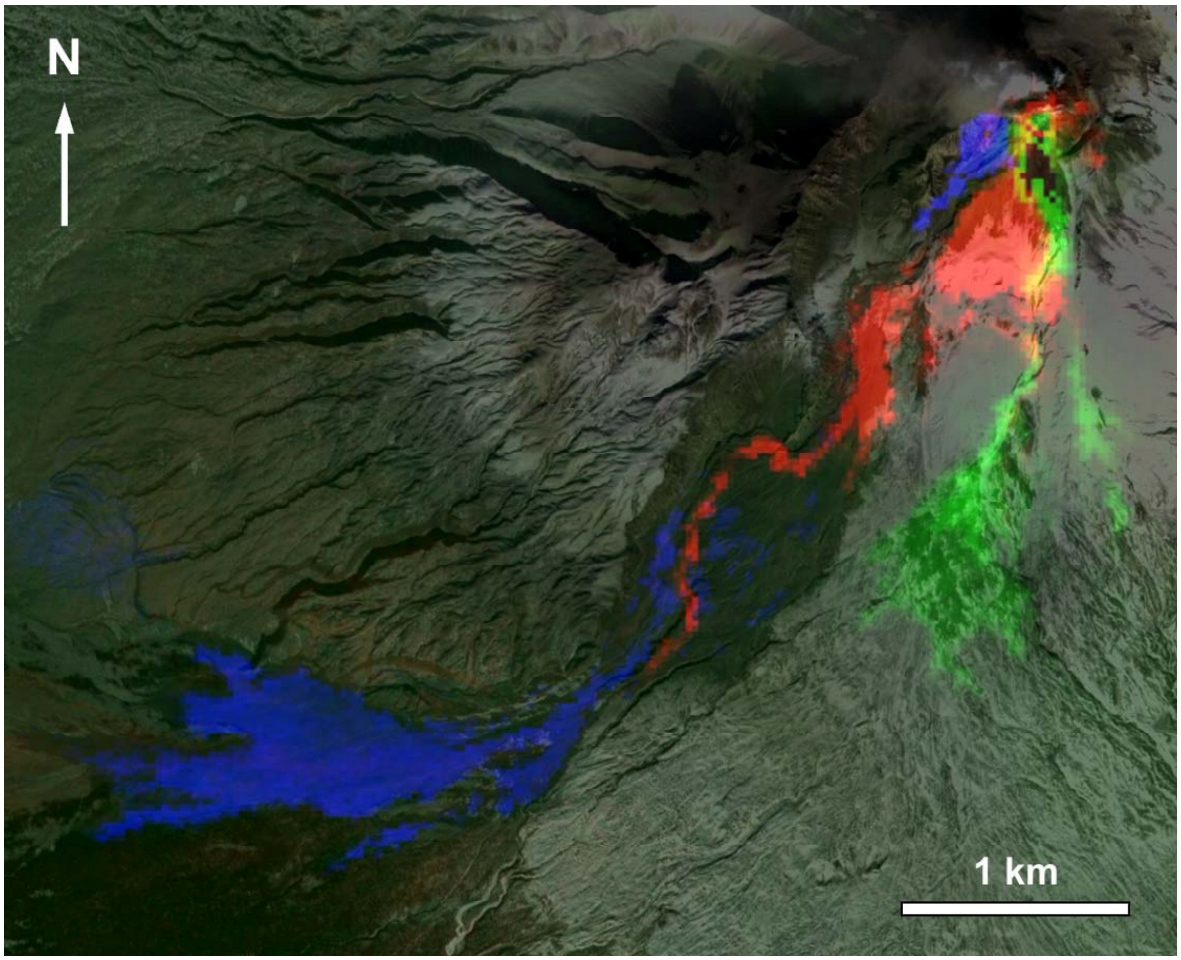

3.3. Multi-Temporal Analysis of ASTER Data: January 2000–January 2009.

Lava dome growth (Figure 1) and the emplacement of pyroclastic flow deposits on its flank has been common at Shiveluch over the study period (2000–present). The ASTER images collected per year were examined, with many of these coming from the urgent request program (Figure 3). Manual requests for ASTER data were also ongoing during times of heightened activity, therefore an increase in the number of images in any given year normally correlates to a larger eruptive event. There has been a steady increase in the number images collected from 2000 to 2009, with more rapid increases in 2002, 2005, and 2007. The peak in the total number of images per year was in 2007, which declined the following year. Clearly, the inception the ASTER Urgent Request Program for volcano monitoring in 2004 was responsible for the increase in the total number of images acquired at Shiveluch (Figure 3).

Figure 3. The record of ASTER images (graphs) and AVHRR (orange diamonds) anomalies observed from 2000 to 2009. The total number of ASTER images are averaged per year, whereas the AVHRR data are listed individually per day. Prior to the inception of the ASTER URP program in 2004 an average of 17 images per year were acquired. Following the URP start, this increased to an average of 40 images per year. The peak in images collected per year was in 2007, which also coincided with highest levels of volcanic activity.

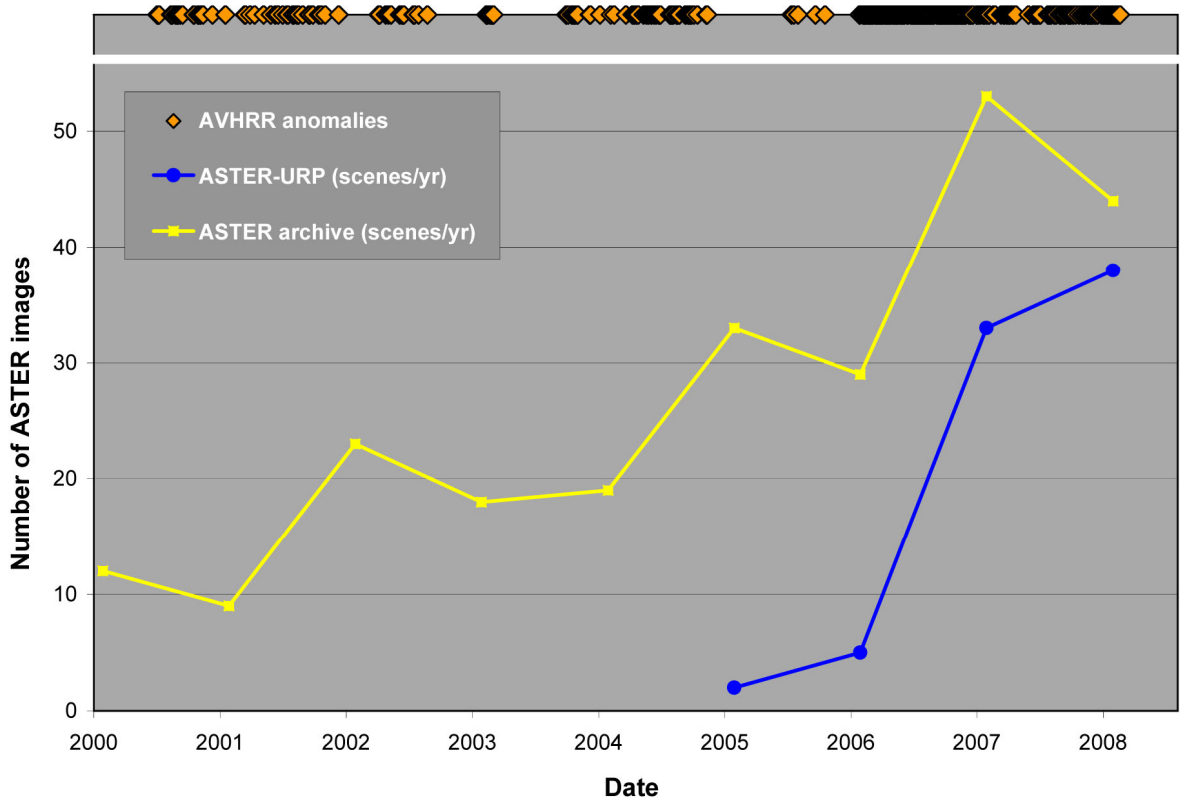

ASTER-derived, Level 2 surface kinetic temperature data were compared to AVHRR thermal anomalies detected over the dome region (Figure 4). The number of AVHRR thermal anomalies were relatively constant over the entire time period, except for three main periods of no or very few anomalies: (1) August 2000–June 2001; (2) July 2003–September 2004; and (3) October 2005–January 2007. From the entire ASTER archive, 27 images were selected that were completely cloud-free over the summit area. The maximum (non-saturated) dome temperature for each scene was extracted and compared to the AVHRR data archive. One time period produced sustained below-average ASTER temperatures: August 2006. This time periods also coincided with a lack of observed AVHRR thermal anomalies. The lower thermal output suggests periods of little to no extrusive activity or very long periods of sustained cloud cover. Such cloud cover would reduce the number of hot spots detected, however this is unlikely. The high temporal frequency of AVHRR typically guarantees a limited number of summit observations even during cloudy periods. Furthermore, the large time periods where no hotspots were detected would suggest that activity levels were significantly reduced during these times. Reports from KVERT also confirm this lack of activity during this time period [24]. This is

especially notable where compared with the nearly constant level of activity after January 2007, during which there has been multiple periods of high cloud cover.

Figure 4. Multi-temporal thermal trends at Shiveluch from 1 January 2000 to 19 January 2009. ASTER-derived maximum pixel-integrated brightness-temperature (blue line) above the average background temperature (yellow line). Data were extracted from the hottest part of the lava dome. AVHRR thermal anomalies (orange diamonds) are shown at the top of the graph along with and the six major explosive eruptions as red triangles (19 May 2001, 9 May 2004, 28 February 2005, 22 September 2005, 29 March 2007, and 18 December 2007).

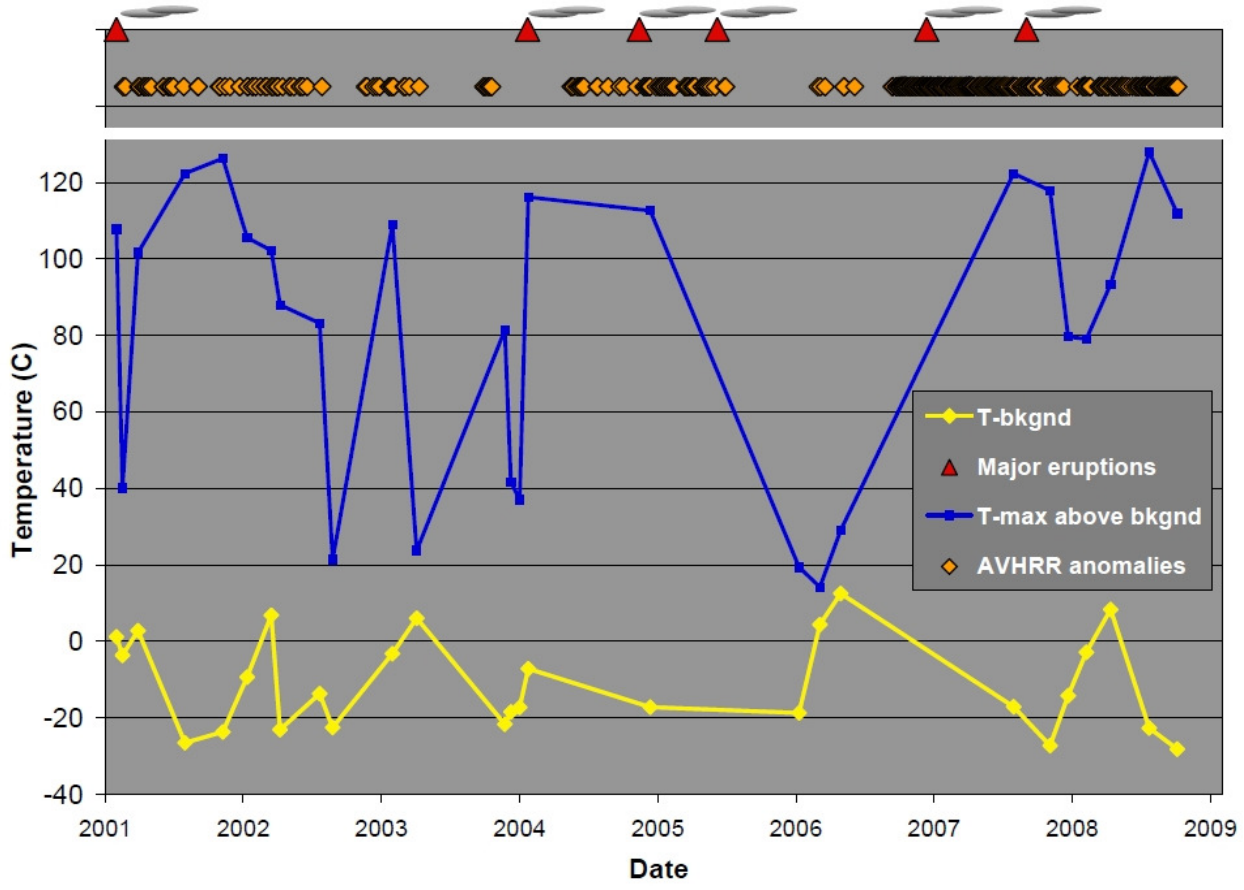

4. Concluding Remarks

The nine year ASTER TIR data archive has been mined and 27 cloud-free scenes were used here to show ongoing thermal and visual observations following three large explosive eruptions at Shiveluch volcano. These periods of activity were well-imaged due to a collaborative program using AVHRR/MODIS data to trigger a higher temporal frequency of ASTER data. The periods of increased volcanic activity produced numerous PF deposits. If such eruptive products were deposited in more populated areas they would have posed a significant risk on the ground. AVHRR data were also used to validate the nine year archive of ASTER-derived temperatures and to detect three periods of minimal thermal output, which denote periods of probable quiescence. Volcanoes on the Kamchatka

Peninsula and in the north Pacific region continue to pose a risk to cargo and passenger aircraft that traverse this region's airspace, highlighting the need for ongoing research and monitoring in this area using both high temporal/low spatial resolution data combined with lower temporal/higher spatial resolution data. Such an approach can also be applied to other volcanoes globally in order to better constrain their activity and more importantly their eruptive behaviour and patterns over the decadal time scale.

Acknowledgements

This research was made possible by NASA (Grants: NNG04GO69G and NNX08AJ91G) and the ASTER Science Team (MSR), the Andrew W. Mellon Foundation (AJC), and the Henry Leighton Memorial Scholarship (AJC). The authors thank Michael Muder for database assistance and acknowledge the advice and help of Olga Girina for her continued assistance with all Kamchatka projects.

References and Notes

1. Fedotov, S.A.; Masurenkov, Yu.P. *Active Volcanoes of Kamchatka*; Nauka: Moscow, Russia, 1991; Volume 1; pp. 168–197.
2. Belousov, A.; Belousova, M.; Voight, B. Multiple edifice failures, debris avalanches and associated eruptions in the Holocene history of Shiveluch volcano, Kamchatka, Russia. *Bull. Volcanol.* **1999**, *61*, 324–342.
3. Menyailov, A.A. Shiveluch volcano, its geological structure, composition and eruptions. *Trans. Volcan. Lab. USSR Acad. Sci.* **1955**, *9*, 294, (in Russian).
4. Melekestsev, I.V.; Volynets, O.N.; Ermakov, V.A.; Kirsanova, T.P.; Masurenkov, Yu.P. Shiveluch Volcano. In *Active Volcanoes of Kamchatka*; Fedotov, S.A., Masurenkov, Yu.P., Eds.; Nauka: Moscow, Russia, 1991; Volume 1, pp. 84–92 (in Russian).
5. Dirksen, O.; Humphreys, M.C.S.; Pletchov, P.; Melnik O.; Demyanchuk Y., Sparks, R.S.J.; Mahony S. The 2001–2004 dome-forming eruption of Shiveluch volcano, Kamchatka: Observation, petrological investigation and numerical modeling. *J. Volcanol. Geotherm. Res.* **2006**, *155*, 201-226.
6. Ponomareva V.V.; Pevzner M.M.; Melekestsev, I.V. Large debris avalanches and associated eruptions in the Holocene eruptive history of Shiveluch volcano, Kamchatka, Russia. *Bull. Volcanol.* **1998**, *59*, 490–505.
7. Belousov, A.B. The Shiveluch volcanic eruption of 12 November 1964—Explosive eruption provoked by failure of the edifice. *J. Volcanol. Geotherm. Res.* **1995**, *66*, 357–365.
8. Fedotov, S.A.; Dvigalo, V.N.; Zharinov, N.A.; Ivanov, V.V.; Seliverstov, N.I.; Khubunaya, S.A.; Demyanchuk, Yu.; Markov, L.G.; Osipenko, L.G.; Smelov, N.P. The eruption of Shiveluch volcano on May–July 2001. *Volcanol. Seismol*. **2001**, *6*, 3–15, (in Russian).
9. Dehn, J.; Dean, K.G.; Engle, K. Thermal monitoring of North Pacific volcanoes from Space. *Geology* **2001**, *28*, 755–758.

10. Duda, K.A.; Ramsey, M.; Wessels, R.; Dehn, J. Optical satellite volcano monitoring: A multi-sensor rapid response system. In *Geoscience and Remote Sensing*; Ho, P.P., Ed.; IN-TECH Press: Vukovar, Croatia, 2009; pp. 473–496.
11. Carter, A.J.; Ramsey, M.S.; Belousov, A.B. Detection of a new summit crater on Bezymianny Volcano lava dome: satellite and field-based thermal data. *Bull. Volcanol*. **2007**, *69*, 811–815.
12. Carter, A.J.; Girina O.A.; Ramsey, M.S.; Demyanchuk, Y. ASTER and field observations of the 24 December 2006 eruption of Bezymianny Volcano, Russia. *Remote Sens. Environ.* **2008**, *112*, 2569–2577.
13. Ramsey, M.S.; Dehn, J.; Wessels, R.; Byrnes, J.; Duda, K.; Maldonado, L.; Dwyer, J. The ASTER emergency scheduling system: A new project linking near-real-time satellite monitoring of disasters to the acquisition of high-resolution remote sensing data. In *Proceedings of AGU Fall Meeting 2004*, San Francisco, CA, USA, 13–17 December 2004; Abstract # SF23A-0026.
14. Ramsey, M.S.; Anderson, S.; Wessels, R. Active dome and pyroclastic flow deposits of Sheveluch Volcano, Kamchatka: Unique thermal infrared and morphologic field observations. In *IAVCEI General Assembly*, Reykjavik, Iceland, August 18–24, 2008; p. 67.
15. Rose, S.R.; Ramsey, M.S. The 2005 eruption of Kliuchevskoi volcano: Chronology and processes derived from ASTER spaceborne and field-based data. *J. Volcanol. Geotherm. Res.* **2009**, doi:10.1016/j.jvolgeores.2009.05.001.
16. Yamaguchi, Y.; Kahle, A.B.; Tsu, H.; Kawakami, T.; Pniel, M. Overview of Advanced Spaceborne Thermal Emission and Reflection Radiometer (ASTER). *IEEE Trans. Geosci. Remote Sens.* **1998**, *36*, 1062–1071.
17. Abrams, M. The Advanced Spaceborne Thermal Emission and Reflectance Radiometer (ASTER): Data products for the high spatial resolution imager on NASA's Terra platform. *Int. J. Remote Sens.* **2000**, *21*, 847–859.
18. Pieri, D.C.; Abrams, M.J. ASTER watches the world's volcanoes: a new paradigm for volcanological observations from orbit. *J. Volcanol. Geotherm. Res.* **2004**, *135*, 13–28.
19. Ramsey, M.S.; Dehn, J. Spaceborne observations of the 2000 Bezymianny, Kamchatka eruption: The integration of high-resolution ASTER data into near real-time monitoring using AVHRR. *J. Volcanol. Geotherm. Res.* **2004**, *135*, 127–146.
20. *ASTER Volcano Database*; Geological Survey of Japan, AIST: Tokyo, Japan, 2009, Available online: http://igg01.gsj.jp/vsidb/image/index-E.html (accessed on 15 November 2010).
21. *Warehouse Inventory Search Tool*; NASA, 2009, Available online: https://wist.echo.nasa.gov/~wist/api/imswelcome/ (accessed on 15 November 2010).
22. Gillespie, A.R.; Rokugawa, S.; Matsunaga, T.; Cothern, J.S.; Hook, S.; Kahle, A.B. A temperature and emissivity separation algorithm for Advanced Spaceborne Thermal Emission and Reflection Radiometer (ASTER) images. *IEEE Trans. Geosci. Rem. Sens.* **1998**, *36*, 1113–1126.
23. Scheidt, S.; Ramsey, M.S.; Lancaster, N. Determining soil moisture and sediment availability at White Sands Dune Field, NM from Apparent Thermal Inertia (ATI) data. *J. Geophys. Res*. **2010**, *115*, F02019, doi:10.1029/2009JF001378.

24. *Shiveluch Volcano*; Bulletin Global Volcanism Network; Smithsonian Institution: Washington, DC, USA, November 2006; Volume 31.